Mechanical stress, fracture risk, and beak evolution in Darwin's ground finches (*Geospiza*).

Joris Soons[1], Anthony Herrel[2,3], Annelies Genbrugge[1,4], Peter Aerts[3,5], Jeffrey Podos[6], Dominique Adriaens[4], Yoni De Witte[7], Patric Jacobs[8] and Joris Dirckx[1]

1. Laboratory of Biomedical Physics, University of Antwerp, Groenenborgerlaan 171, B-2020 Antwerpen, Belgium.
2. Département d'Ecologie et de Gestion de la Biodiversité, Museum National d'Histoire Naturelle, 57 rue Cuvier, Case postale 55, 75231, Paris Cedex 5, France.
3. Department of Biology, University of Antwerp, Universiteitsplein 1, 2610 Antwerpen, Belgium.
4. Evolutionary Morphology of Vertebrates, Ghent University – UGent, K.L. Ledeganckstraat 35, 9000 Gent, Belgium.
5. Department of Movement and Sports Sciences, Ghent University, Watersportlaan 2, 9000 Gent, Belgium.
6. Department of Biology and Graduate Program in Organismic and Evolutionary Biology, University of Massachusetts, Amherst MA 01003, USA.
7. Department of Subatomic and Radiation Physics, Ghent University – UGent, Proeftuinstraat 86, 9000 Gent, Belgium.
8. Department of Geology and Soil Science, University of Ghent, Krijgslaan 281/S8, B-9000 Gent, Belgium.

pages: 14; # figures: 3; # tables: 1

Address for correspondence:

Anthony Herrel

Département d'Ecologie et de Gestion de la Biodiversité,

57 rue Cuvier,

Case postale 55,

75231 Paris

France

phone: ++33-140798120

e-mail: anthony.herrel@mnhn.fr

Abstract

Darwin's finches have radiated from a common ancestor into fourteen descendent species, each specializing on distinct food resources and evolving divergent beak forms. Beak morphology in the ground finches (*Geospiza*) has been shown to evolve via natural selection in response to variation in food type, food availability, and interspecific competition for food. From a mechanical perspective, however, beak size and shape are only indirectly related to birds' abilities to crack seeds, and beak form is hypothesized to evolve mainly under selection for fracture-avoidance. Here we test the fracture-avoidance hypothesis using finite element modeling. We find that across species, mechanical loading is similar and approaches reported values of bone strength, thus suggesting pervasive selection on fracture-avoidance. Additionally, deep and wide beaks are better suited for dissipating stress than are more elongate beaks when scaled to common sizes and loadings. Our results illustrate that deep and wide beaks in ground finches enable reduction of areas with high stress and peak stress magnitudes, allowing birds to crack hard seeds while limiting the risk of beak failure. These results may explain strong selection on beak depth and width in natural populations of Darwin's finches.

Key words: Darwin's Finches, finite element modeling, bite force, beak shape

1. INTRODUCTION

Beak morphology in Darwin's finches has been shown to evolve via natural selection in response to variation in food type, food availability, and interspecific competition for food (Lack 1947; Grant 1999; Grant & Grant 2006). Consequently, divergent beak sizes and shapes evolved in Darwin's finches specializing on different food items (Lack 1947; Bowman 1961; Grant 1999; Foster et al. 2008). Variation in beak shape in the ground finches of the genus *Geospiza* is situated mainly along two axes: variation in width and depth which co-vary, and variation in length (Bowman, 1961). Species that crush hard seeds at the base of their beaks, such as *G. fortis* and *G. magnirostris* tend to have relatively short but wide and deep beaks (Grant 1999). Other species, such as *G. scandens* and *G. difficilis* tend to have longer yet narrower and shallower beaks, a design that has been suggested to be a compromise between base-crushing and probing (Bowman 1961). Interestingly, the two principal axes of variation observed within the ground finch clade are also reflected in distinct developmental pathways (Abzhanov et al. 2004, 2006).

While much research has focused on beak size and shape, the seed cracking ability of a bird is determined more directly by bite force capacity which is, in turn, closely dependent on jaw adductor muscle cross sectional area (Bowman 1961; Van der Meij & Bout 2004; Herrel et al. 2005a, b). The jaw closer muscles, situated at the back of the head, generate crushing forces that are transferred to food by means of the upper and lower beak (Herrel et al. 2005a, b). Beak morphology is thus expected to evolve in concert with jaw adductor force generation capacity, through selection for the capacity to avoid structural failure under conditions of increased muscle and food reaction forces (Bowman 1961). Indeed, almost 50 years ago Bowman (1961) suggested that the shape of the beak was adapted for fracture resistance, with beaks with more or less straightened culmen or gonys (upper and lower beak respectively) tending to reduce fracture risk. Modifications towards increased beak depth, on the other

hand, were interpreted as adaptations towards more powerful crushing bites (Bowman 1961).

To test these hypotheses, we developed finite element models (FEM) of the upper beak in ground finches (Table 1). As finite element models quantify the effect of complex shape variation on stress magnitude and distribution (Richmond et al. 2005; Ross 2005; Rayfield 2007; Rayfield & Milner 2008), they are ideally suited to address the hypothesis that beak shape has evolved in response to fracture avoidance, and may also offer insights into observed patterns of selection on beak shape (depth, width and curvature) in species that crack hard seeds.

2. MATERIAL AND METHODS

(a) *Fresh specimens and muscle data*

Road-killed specimens were collected during February-March of 2005 and 2006 on Santa Cruz Island, under a salvage permit from the Galápagos National Park Service. Intact specimens were collected and preserved in a 10% aqueous formaldehyde solution for 24 hours, rinsed and transferred to a 70% aqueous ethanol solution. Specimens were transported to Belgium where one individual each of *G. fortis*, *G. fuliginosa*, and *G. scandens* was scanned at the Ghent University CT-scanning facility. A second specimen of each of these species was dissected and all jaw muscle bundles removed individually. Muscles were blotted dry and weighed on a Mettler microbalance (± 0.01mg). Next, muscles were transferred individually to petri dishes and submerged in a 30% aqueous nitric acid solution for 18 hours to dissolve all connective tissue (Loeb & Gans 1986). After removal of nitric acid, muscles were transferred to a 50% aqueous glycerol solution and fibers teased apart using blunt-tipped glass needles. Next, 30 fibers were selected and drawn using a binocular scope with attached camera lucida. A background grid was also drawn in each image to provide an object for scaling.

Drawings were scanned and fiber lengths determined using Scion Image (freely available at http://www.scioncorp.com).

Based on the muscle mass and fiber lengths, the physiological cross sectional area of each muscle bundle was determined assuming a muscle density of 1060 kg/m^3 (Méndez & Keys 1960). Since pennate muscles were separated into their individual bundles, no additional correction for pennation angle was included. Force generation capacity for each muscle was calculated assuming a muscle stress of 30 N/cm^2 (Nigg & Herzog 1999). As the external adductor and pseudotemporalis muscle bundles act only indirectly on the upper beak through the jugal bone (Nuijens & Zweers 1997; van der Meij & Bout 2004), the component of the muscle force transferred to the upper beak was calculated by taking into account the position of the muscles and the angle thereof relative to the jugal bone. The pterygoid muscle bundles, by contrast, act directly on the upper beak (Nuijens & Zweers 1997; van der Meij & Bout 2004) and muscle forces were assumed to be directly transmitted through the pterygoid/palatine complex.

(b) *CT scanning and reconstruction*

Road-killed specimens of *G. fortis*, *G. fuliginosa* and *G. scandens* were scanned at the UGCT scanning facility (www.ugct.ugent.be), using a micro-focus directional type X-ray tube, set at a voltage of 80 kVp and a spot size of 10 micrometer. Specimens were mounted on a controllable rotating table (MICOS, UPR160F-AIR). For each specimen a series of 1000 projections of 940x748 pixels was recorded covering 360 degrees resulting in voxel sizes of 43.73 µm for *G. fortis*, 34.84 µm for *G. fuliginosa*, and 42.77 µm for *G. scandens*. Reconstruction of the tomographic projection data was done using the Octopus-package (Vlassenbroeck et al. 2007).

Specimens of *G. difficilis* (MCZ39828) and *G. magnirostris* (MCZ65745) were scanned at the Harvard CNS facility using an X-Tek XRA-002 micro-CT imaging

system set at 75KV. Specimens were mounted on a rotating table and a series of 3142 projections of 2000 by 2000 pixels covering 360 degrees was recorded resulting in voxel sizes of 25.26 µm for *G. difficilis*, and 45.75 µm for *G. magnirostris*. Reconstruction of the tomographic projections was done using CTPro (Metris) and VGStudio Max 2.0 (Volume Graphics). Volume and surface rendering was performed using Amira 5.0 (64-bit version, Computer Systems Mercury) for all specimens.

(c) *Finite Element Modeling*

CT image sequences were segmented semi-automatically based on grayscale thresholding and smoothed using Amira 5.0 (64-bit version, Computer Systems Mercury), to obtain a triangular surface mesh of the upper beak (Fig. 1). Next, a Delaunay tetrahedral volume mesh with a minimum radius-edge ratio of 1.4 was generated in tetgen (Si 2008) and imported in the finite element program FEBio (Maas and Weiss 2008). A left unilateral load with all muscles bilaterally activated to 100% was applied at a posterior bite point, the position of which was determined based on recordings of birds cracking seeds in the field. For each modeled specimen, the bite point was simulated through a translation constraint of the corresponding elements. The fronto-nasal hinge was modeled as two rotating but fixed elements. The forces on palatine and jugal bones were applied along the long axis of these bones as determined on the CT-data, and with a magnitude derived from calculated muscle forces. Bone was modeled as a linear elastic, isotropic and homogeneous material with a Young's modulus from 18 GPa, and a Poisson ratio of 0.3 (Yamada 1970; Evans 1973; Vogel 2003; Currey 2006). Linear elements were used in the models, which were solved with an iterative Newton-based Broyden-Fletcher-Goldfarb-Shanno (BFGS) solver. The convergence and the stability of the results were tested by an iterative refinement of the mesh up to 500,000 elements and terminated at an accuracy of 5% or better.

As stress is a complex three-dimensional phenomenon, inherently difficult to interpret, we chose to combine the stresses using the Von Mises criterion. Three areas with high stress were noted in our simulations: posterior on the maxilla in front of the nasal apertures, and on the ipsi- and contra-lateral processi maxillari of the nasal bone. A high stress area posterior on the beak was not considered as high stresses in this region may be due to constraints imposed at the fronto-nasal hinge. The maximal Von Mises stress observed in a volume with a predefined radius was recorded in all areas showing high stress, and compared across loading conditions for the different species (Table 1). Peak stress values were recorded in meshes of increasing complexity allowing us to test the convergence of the model solution (see Herrel et al. in press). Additionally, the external force needed to satisfy the constraint at the bite point, perpendicular to the surface area, was calculated and the magnitude thereof was recorded and compared to the bite forces measured *in vivo* (Table 1). Finally, FE-models for *G. difficilis*, *G. fuliginosa*, *G. magnirostris*, and *G. scandens* were scaled by model area (see Dumont et al. 2009) to the same size as the *G. fortis* model, and simulations were run with input forces based on *G. fortis* in order to evaluate how beak shape affects loading of the beak.

3. RESULTS

The three species of Darwin's finch featured in our analysis showed a nearly three-fold absolute difference in the cross sectional area of the jaw adductor muscles (0.28 mm^2 in *G. fuliginosa* versus 0.72 mm^2 in *G. fortis*), and thus also in the maximal potential loading of the beak. A first set of FEM simulations was performed using actual beak size and shape as determined from CT scans, and applied input forces based on information derived from muscle dissections for the three species for which specimens were available for dissection. Results from these simulations show that beaks in all species show stress concentrations in similar regions, specifically in the region of the nasal bone posterior to the nasal aperture, and in the processi maxillari of the nasal bone (Fig. 2). Stresses were

typically highest at the dorsal and posterior aspect of the nasal bone and at the processus maxillaris contra lateral to the bite side (Fig. 2, Table 1).

A second set of FEM simulations was performed in which beaks were scaled to the area of the *G. fortis* specimen, and then loaded using the input forces calculated for this species (Fig. 3). This was done to characterize the potential effects of beak shape variation on force dissipation. If interspecific variation in beak shape does not impact force dissipation, all simulations would show comparable stress distributions and stress magnitudes. In contrast, the results identify marked differences among species in stress distributions, thus demonstrating the importance of beak shape in force dissipation. Species with elongate beaks such as *G. scandens* and *G. difficilis* show notable increases in the surface area subjected to high stress, spreading forward to the dorsal aspect, anterior of the nasal aperture. Moreover, the peak stresses calculated for the species with the longer and narrower beaks (*G. scandens* and *G. difficilis*; Table 1) were substantially higher (max. of 72 MPa). In contrast, the tall and wide beaks as seen in *G. fortis*, *G. fuliginosa*, and *G. magnirostris* are seen to distribute the load applied to the beak with lower peak stress values (max. of 44 MPa across the three species), largely confined to the posterior aspect of the nasal bone. Note, however, how an additional area of high stress in the *G. magnirostris* model is present at the level of the bite point.

4. DISCUSSION

A comparison of the bite forces calculated in our FEMs with actual bite forces measured *in vivo* (Table 1) shows that calculated values fall within the *in vivo* range, thus confirming that our models provide realistic estimates of beak loadings. Interestingly, our results provide one of the few cases where the output of FEMs is validated against *in vivo* data and suggest that FEMs can provide realistic output if based on realistic inputs (see Rayfield 2007 for an overview; Kupczik et al. 2009; Strait et al. 2009). However, our models must be considered as only a first step, and planned future models including the keratinous

rhamphotheca and material properties for the beaks of Darwin's finches are needed to test whether a refinement of our models affects the output of our FE models in terms of stress distributions and magnitudes. Additionally, analyses of how constraints and loading conditions affect stress magnitudes and distributions in beaks with different morphologies are needed and currently underway (see Herrel et al. in press).

A comparison of peak stresses reported here in the different species of Darwin's finch with values reported for the compressive strength of bone suggests that Darwin's finch beaks operate with safety factors between 3 and 5 in most species, assuming an average compressive bone strength of 165 MPa (note that bone strength ranges from 106-224 MPa across a wide range of vertebrates; Yamada 1970; Vogel 2003; Currey 2006). However, it should be noted that these are conservative estimates of safety factors as bone is known to fail in tension at much lower stresses (e.g. 117MPa; Evans 1973). However, without specific data on material properties for the beaks of the birds considered here this must remain speculative to some degree. Moreover, Von Mises stress is often considered to be one of the best predictors of bone failure (Keyak & Rossi 2000), making it an appropriate value to use in the calculation of safety factors. Previously it was suggested that beak morphology should evolve in concert with the force generating capacity of the jaw adductors through selection for the capacity to avoid structural failure under conditions of increased muscle and food reaction forces (Bowman 1961). Our data support this assertion and suggest that beaks are indeed optimized to withstand their natural loading regimes.

Almost five decades ago Bowman (1961) suggested that the shape of the beak in Darwin's finches was related to fracture resistance, such that beaks with a more or less straightened culmen and gonys (the upper and lower beak respectively) tend to reduce fracture risk. Modifications towards increased beak depth, on the other hand, were interpreted as adaptations towards a more powerful crushing bite (Bowman 1961). Our data provide only partial support for these hypotheses. Whereas deeper and wider beaks indeed appear better suited

to withstand reaction forces from biting and may thus allow for higher bite forces, the straighter beaks of *G. scandens* and *G. difficilis* clearly induce greater stresses, thus presumably increasing fracture risk. The difference between *G. difficilis* and *G. fuliginosa* is especially notable, with the highest peak Von Mises stress in *G. difficilis* being almost twice that of *G. fuliginosa* when scaled to the same surface area. Interestingly, however, the beak with the greatest curvature in *G. magnirostris* is seen to perform somewhat poorer than that of *G. fuliginosa* when scaled to the same surface area, suggesting that too much curvature may negatively affect stress magnitudes as predicted by Bowman (1961). Alternatively, the relatively high stress may be due to the relatively low volume (and thus bone present) of the upper beak of the *G. magnirostris* specimen used in our models (see Table 1). As this specimen and the *G. difficilis* used are dried historical specimens, this may represent a preservation artifact and thus results for both *G. difficilis* and *G. magnirostris* should be interpreted with caution. Testing for potential preservation artifacts will require freshly preserved specimens, which may prove to be difficult to obtain.

In summary, our results illustrate that deep and wide beaks in Darwin's finches, long associated with an ability to crack hard seeds, more specifically limit beak areas that experience high stress and peak stress magnitudes. Consequently, deep and wide beaks may allow birds to crack hard seeds while limiting the risk of beak failure. Deeper beaks are indicative of deeper dorsal nasal regions, and wider beaks indicative of a broader maxillary process of the nasal bone, the two areas typically showing high stress concentrations in our model. Thus, our simulations may help explain the low survival of birds with smaller beaks in times of food scarcity when seeds of intermediate size are rapidly depleted from the environment (Boag & Grant 1981). Given the often large within-population variation in beak size and shape (Grant 1983; Grant 1999; Grant & Grant 2006), birds with relatively smaller (more narrow or shallow) beaks for a given jaw adductor size may be subject to mechanical failure more rapidly under the repeated loading needed to crack hard seeds such as *Tribulus* (Grant 1981)

which are relatively abundant during dry years (Grant 1999). Finally, our data show how jaw musculature and beak shape have co-evolved in Darwin's finches that specialize on different food resources. We suggest that finch jaw musculature and its relationship to beak safety factors is as critical in finch evolution and adaptive radiation as is the evolution of the beak morphology itself. Future modeling efforts including other radiations of birds specializing on cracking seeds will be crucial to test the generality of our results.

Acknowledgements

We thank S. Maas and J Weis (University of Utah) for allowing us to use the FEBio software package. Field work was coordinated through the Charles Darwin Research Station and the Galápagos National Park Service. The authors thank Luis De Leon, Ana Gabela, Katleen Huyghe, Andrew Hendry, Mike Hendry, Eric Hilton, Sarah Huber, and Bieke Vanhooydonck for their assistance in the field and for helping collect road killed specimens. This work was performed in part at the Center for Nanoscale Systems (CNS), a member of the National Nanotechnology Infrastructure Network (NNIN), which is supported by the National Science Foundation under NSF award no. ECS-0335765. CNS is part of the Faculty of Arts and Sciences at Harvard University. Supported by NSF grant IBN-0347291 to J.P., by an interdisciplinary research grant of the special research fund of the University of Antwerp to PA, JD, JS, AG and AH, and by an Aspirant fellowship of the Research Foundation – Flanders to JS. The UGCT scanning facility acknowledges the support from the Ghent University special research fund (BOF).

REFERENCES

Abzhanov, A., Protas, M., Grant, R. B., Grant, P. R. & Tabin C. J. 2004. Bmp4 and morphological variation of beaks in Darwin's finches. *Science* **305**, 1462-1465.

Abzhanov, A., Kuo, W. P., Hartmann, C., Grant, B. R., Grant, P. R. & Tabin C. J. 2006. The calmodulin pathway and evolution of elongated beak morphology in Darwin's finches. *Nature* **442**, 563-567.

Boag, P. T. & Grant, P. R. 1981. Intense natural selection in a population of Darwin's finches (Geospizinae) in the Galapagos. *Science* **214**, 82-85.

Bowman, R. I. 1961. Morphological differentiation and adaptation in the Galapagos finches. *Univ. Calif. Publ. Zool.* **58**, 1-302.

Currey, J. D. 2006. *Bones: structure and mechanics*. Princeton: Princeton University Press.

Dumont, E. R., Grosse, I. R. & Slater, G. J. 2009. Requirements for comparing the performance of finite element models of biological structures. *J. Theor. Biol.* **256**, 96-103.

Evans, F. G. 1973. Mechanical properties of bone. Springfield: Charles C. Thomas.

Foster, D., Podos, J. & Hendry, A. P. 2008. A geometric morphometric appraisal of beak shape in Darwin's finches. *J. Evol. Biol.* **21**, 263-275.

Grant, P. R. 1981. The feeding of Darwin's Finches on *Tribulus cistoides* (L.) seeds. *Anim. Behav.* **29**, 785-793.

Grant, P. R. 1983. Inheritance of size and shape in a population of Darwin's finches, *Geospiza conirostris*. *Proc. R. Soc. Lond. B* **220**, 219-236.

Grant, P. R. 1999. *The Ecology and Evolution of Darwin's Finches*. Princeton: Princeton University Press.

Grant, P. R. & Grant, B. R. 2006. Evolution of character displacement in Darwin's Finches. *Science* **313**, 224-226.

Herrel, A., Podos, J., Huber, S. K. & Hendry, A. P. 2005a. Evolution of bite force in Darwin's finches: a key role for head width. *J. Evol. Biol.* **18**, 669-675.

Herrel, A., Podos, J., Huber, S. K. & Hendry, A. P. 2005b. Bite performance and morphology in a population of Darwin's finches: implications for the evolution of beak shape. *Funct. Ecol.* **19**, 43-48.

Herrel, A., Soons, J., Aerts, P., Dirckx, J., Boone, M., Jacobs, P., Adriaens, D. & Podos, J. in press. Adaptation and function of Darwin's finch beaks: divergence by feeding type and sex. *Emu*.

Keyak, J. H. & Rossi, S. A. 2000. Prediction of femoral fracture load using finite element models: an examination of stress- and strain-based failure models. *J. Biomech.* **33**, 209-214.

Kupczik, K., Dobson, C., Phillips, R., Oxnard, C., Fagan, M & O'Higgins, P. 2009. Masticatory loading and bone adaptation in the supraorbital torus of developing macaques. *Am. J. Phys. Anthropol.* **139**, 193-203.

Lack, D. 1947. *Darwin's Finches*. Cambridge: Cambridge University Press.

Loeb, G. E. & Gans, C. 1986. *Electromyography for experimentalists*. Chicago: University of Chicago Press.

Maas, S. & Weiss, J. A. 2008. FEBio: Finite Elements for Biomechanics. User's Manual, Version 1.0. http://mrl.sci.utah.edu/uploads/FEBio_um.pdf.

Méndez, J. & Keys, A. 1960. Density and composition of mammalian muscle. *Metabolism* **9**, 184-188.

Nigg, B. M. & Herzog, W. 1999. *Biomechanics of the musculo-skeletal system*. New York: Wiley.

Nuijens, F. W. & Zweers, G. A. 1997. Characters discriminating two seed husking mechanisms in finches (Fringillidae: Carduelinae) and estrildids (Passeridae: Estrildinae). *J. Morphol.* **232**, 1-33.

Rayfield, E. J. 2007. Finite element analysis and understanding the biomechanics and evolution of living and fossil organisms. *Annu. Rev. Earth Planet. Sci.* **35**, 541-576.

Rayfield, E. J. & Milner, A. C. 2008. Establishing a framework for archosaur cranial mechanics. *Paleobiology* **34**, 494-515.

Richmond, B. G., Wright, B. W., Grosse, I., Dechow, P. C., Ross, C. F., Spencer, M. A. & Strait, D. S. 2005. Finite-element analysis in functional morphology. *Anat. Rec.* **283A**, 259-274.

Ross, C. F. 2005. Finite-element modeling in vertebrate biomechanics. *Anat. Rec.* **283A**, 253-258.

Si, H. 2008. TetGen: A quality tetrahedral mesh generator and three-dimensional Delaunay triangulator. (http://tetgen.berlios.de)

Strait, D. S., Weber, G. W., Neubauer, S., Chalk, J., Richmond, B. G., Lucas, P. W., Spencer, M. A., Schrein, C., Wright, B. W., Ross, C. F., Dechow, P. C., Wang, Q., Grosse, I., Byron, C., Wood, B. A., Lawn, B., Constantino, P., Slice, D. E., Smith, A. L. 2009. The feeding biomechanics and dietary ecology of *Australopithecus africanus*. *Proc. Natl. Acad. Sci. USA* **106**, 2124-2129.

Van der Meij, M. A. A. & Bout, R. G. 2004. Scaling of jaw muscle size and maximal bite force in finches. *J. Exp. Biol.* **207**, 2745-2753.

Vlassenbroeck, J., Dierick, M., Masschaele, B., Cnudde, V., Van Hoorebeke, L. & Jacobs, P. 2007. Software tools for quantification of X-ray microtomography at the UGCT. *Nuclear Inst. and Methods in Physics Research (A)* **580**, 442-445.

Vogel, S. 2003. *Comparative biomechanics: life's physical world*. Princeton: Princeton University Press.

Yamada, H. 1970. *Strength of biological materials*. Baltimore: Williams and Wilkins.

Figure legends

Figure 1: Schematic overview of the model derivation and methods. **a)** Lateral view of a 3-D reconstruction of the skull of a medium ground finch (*Geospiza fortis*) based on micro CT scans. When birds bite, forces are transmitted by the jaw muscles to the upper beak (blue) via the jugal bones (green) and the pterygoid-palatine complex (orange). The colored zone labeled 1 represents the dorsal nasal region, and the zone labeled 2 represents the maxillary process of the nasal bone. **b)** photograph of the head of a *G. fortis* specimen, skin removed, illustrating the major jaw closing muscles. The external adductor muscles (1, 2) and the m. pseudotemporalis (3) transmit force to the upper beak through the jugal bone. The pterygoideus muscles (4) directly pull the upper beak downward through the pterygoid-palatine complex. **c)** posterior oblique view of the head (left) and upper beak (right) of a *G. fortis*, illustrating loadings and constraints used in the finite element models. Red zones indicate the dorsal constraints on the rotating fixed elements, the yellow circle indicates the bite point (left side), and green arrows indicate the orientation of the load acting on the jugals and palatines.

Figure 2: Output of finite element analyses performed for three different species of ground finches (*Geospiza*) for which specimens were available for dissection. Input forces were calculated from muscle mass and fibre length measurements. Colors indicate calculated resultant Von Mises stresses on the beak in dorsal (left) and lateral (right) views. Warmer colors depict higher stresses. For all species, maximum stress concentration occurs at the posterior part of the nasal bone, posterior to the nasal aperture (zone 1 in Fig. 1a), and within the maxillary

processes of the nasal bone (zone 2 in Fig. 1a). Arrows depict calculated bite forces.

Figure 3: Output of a finite element simulation, in which beak the surface area of the five species of ground finch were scaled to a common surface area (that of *G. fortis*) prior to calculations, and in which the input force calculated for *G. fortis,* was applied to all species. This simulation enables the evaluation of the effects of beak shape on stress distribution. The relatively long and slender beaked *G. scandens* and *G. difficilis* showed disproportional increases in the magnitude of the Von Mises stress and the distribution of areas with high stress (Table 1).

Table 1: Calculated bite force, measured bite force, and output of finite element models.

species	scaled model volume (mm^3)	calculated bite force (N)	measured bite force (N)	peak Von Mises' stress real loading (MPa)			peak Von Mises' stress *G. fortis* loading (MPa)		
				dorsal nasal	ipsilateral max. proc	contralateral max. proc.	dorsal nasal	ipsilateral max. proc.	contralateral max. proc.
G. fortis	112	28.5	26.6 ± 6.5	31.0	41.0	42.0			
G. fuliginosa	120	5.6	4.7 ± 1.5	19.8	24.2	25.2	30.2	35.9	38.7
G. scandens	108	8.4	7.2 ± 1.6	32.9	44.6	32.9	42.6	50.8	61.2
G. magnirostris	89						35.3	42.9	43.9
G. difficilis	66						53.6	49.7	71.5

Bite forces calculated based on the morphology of the specimens and the finite element model, bite forces measured in the field (10), and peak Von Mises stress at three locations on the upper beak showing high stress concentrations (Fig.1). Von Mises stresses were calculated in two simulations; first, with the model loaded using the forces associated with each beak type (Fig. 2), and second when all beaks were scaled to the area of, and loaded with the forces of *G. fortis* (Fig. 3). Max. proc. = maxillary process of the nasal bone (zone 2 in Fig 1a); ipsilateral side = bite side (left); contralateral side = opposite side (right).

Table 1: Calculated bite force, measured bite force, and output of finite element models.

species	scaled model volume (mm^3)	calculated bite force (N)	measured bite force (N)	peak Von Mises' stress real loading (MPa)			peak Von Mises' stress *G. fortis* loading (MPa)		
				dorsal nasal	ipsilateral max. proc	contralateral max. proc.	dorsal nasal	ipsilateral max. proc.	contralateral max. proc.
G. fortis	112	28.5	26.6 ± 6.5	31.0	41.0	42.0			
G. fuliginosa	120	5.6	4.7 ± 1.5	19.8	24.2	25.2	30.2	35.9	38.7
G. scandens	108	8.4	7.2 ± 1.6	32.9	44.6	32.9	42.6	50.8	61.2
G. magnirostris	89						35.3	42.9	43.9
G. difficilis	66						53.6	49.7	71.5

Bite forces calculated based on the morphology of the specimens and the finite element model, bite forces measured in the field (10), and peak Von Mises stress at three locations on the upper beak showing high stress concentrations (Fig.1). Von Mises stresses were calculated in two simulations; first, with the model loaded using the forces associated with each beak type (Fig. 2), and second when all beaks were scaled to the area of, and loaded with the forces of *G. fortis* (Fig. 3). Max. proc. = maxillary process of the nasal bone (zone 2 in Fig 1a); ipsilateral side = bite side (left); contralateral side = opposite side (right).

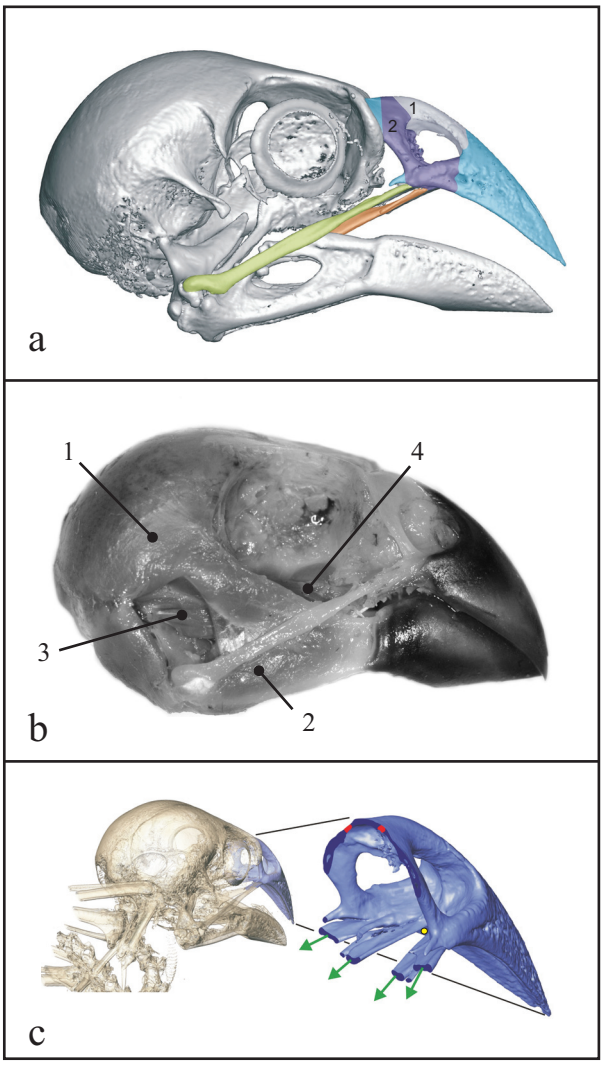
1
2
a
1
4
3
2
b
c

G. fortis

G. fuliginosa

G. scandens

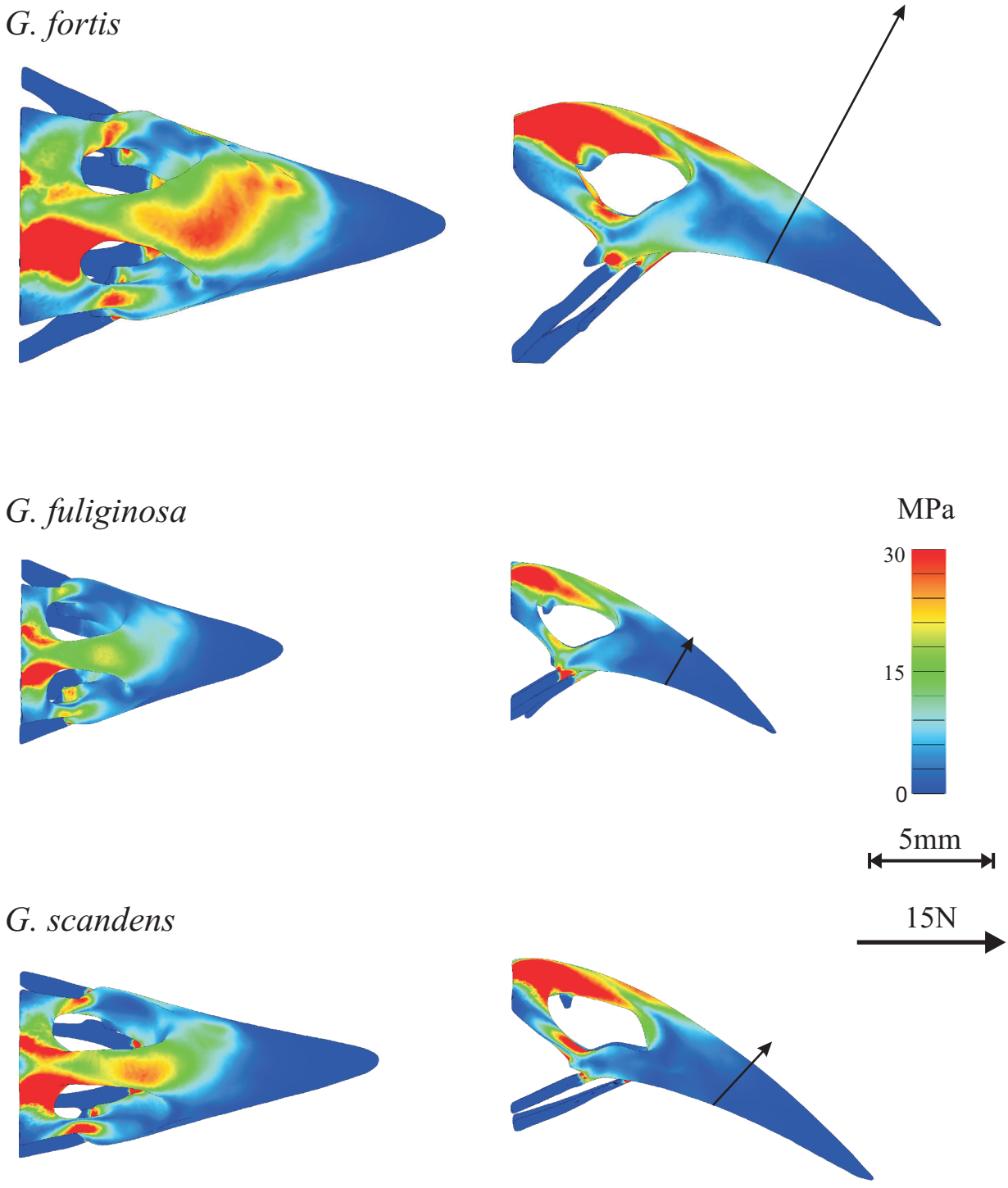

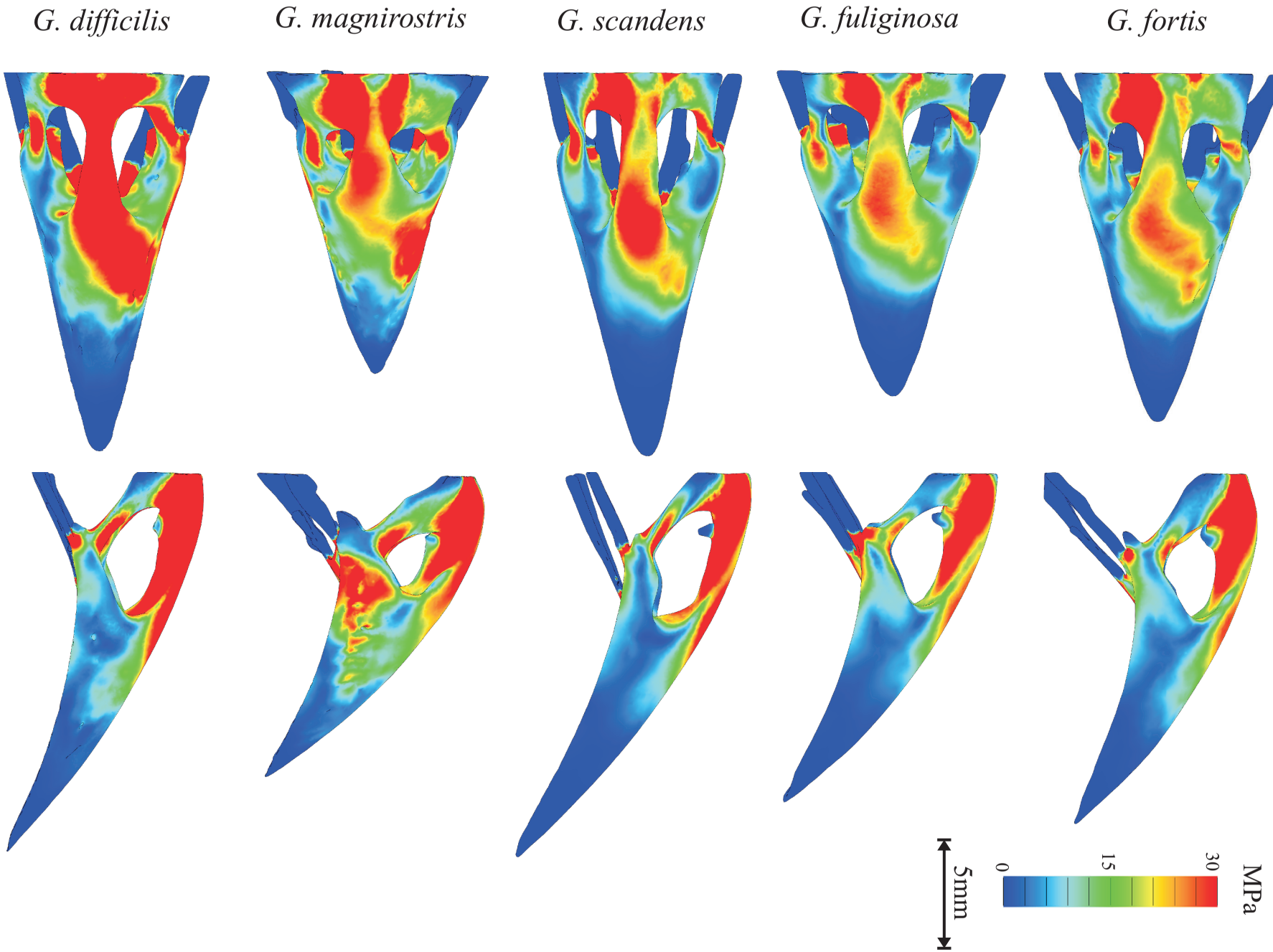
G. difficilis
G. magnirostris
G. scandens
G. fuliginosa
G. fortis
5mm
0
15
30
MPa